

Role of center vortices in chiral symmetry breaking in SU(3) gauge theoryPatrick O. Bowman,¹ Kurt Langfeld,² Derek B. Leinweber,³ André Sternbeck,^{3,4}
Lorenz von Smekal,^{3,5} and Anthony G. Williams³¹*Centre for Theoretical Chemistry and Physics, and Institute of Natural Sciences, Massey University (Albany),
Private Bag 102904, North Shore MSC, New Zealand*²*School of Maths & Stats, University of Plymouth, Plymouth, PL4 8AA, England*³*Centre for the Subatomic Structure of Matter (CSSM), School of Chemistry & Physics, University of Adelaide 5005, Australia*⁴*Institut für Theoretische Physik, Universität Regensburg, D-93040 Regensburg, Germany*⁵*Institut für Kernphysik, Technische Universität Darmstadt, D-64289 Darmstadt, Germany*

(Received 25 October 2010; published 4 August 2011)

We study the behavior of the AsqTad quark propagator in Landau gauge on SU(3) Yang-Mills gauge configurations under the removal of center vortices. In SU(2) gauge theory, center vortices have been observed to generate chiral symmetry breaking and support the infrared behavior of the quark propagator. In contrast, we report a weak dependence on the vortex content of the SU(3) gauge configurations, including the survival of dynamical mass generation on configurations with vanishing string tension.

DOI: [10.1103/PhysRevD.84.034501](https://doi.org/10.1103/PhysRevD.84.034501)

PACS numbers: 12.38.Gc, 11.15.Ha, 12.38.Aw

I. INTRODUCTION

The strong nuclear force has two key features: the dynamical breaking of chiral symmetry ($D\chi SB$) and the confinement of color-charged states. It is tempting to attribute these two phenomena to a single underlying mechanism, an idea supported by finite-temperature studies where the deconfinement and chiral restoration transitions are observed to occur at similar temperatures [1–3]. Low-lying modes of the quark operator, known to dominate $D\chi SB$, are also correlated with the finite-temperature transition of the Polyakov loop, and hence confinement [4–7].

Over the recent past, evidence has been accumulated by means of lattice gauge theories that both phenomena are caused by certain low-energy degrees of freedom. In specific gauges, these degrees of freedom appear as color-magnetic monopoles [8–10] or center vortices [11–13]. The idea that center fluxes disorder Wilson loops, and therefore lead to confinement, is an old one [14,15] and over the last couple of decades a great deal of work has been done in lattice gauge theory on such objects, principally in SU(2) Yang-Mills theory. It turned out to be difficult to define the vortex content of Yang-Mills theory in a physically sensible way. It took until the late '90s until a successful definition was given [16] and the relevance of vortices in the continuum limit was established [17]. The recovery of the string tension from “vortex-only” SU(2) gauge configurations (i.e., Z_2 projected from SU(2)) was shown [11–13], the finite-temperature deconfinement transition was understood in terms of vortex properties [18–21] and a connection to $D\chi SB$ was discovered [22–25].

The use of Landau-gauge Green’s functions as probes of $D\chi SB$ and confinement is an active area of research (see, e.g., [26,27] for a review). It is known, for example, that the gluon propagator violates spectral positivity, which is consistent with gluon confinement [28–30]. In the quark

propagator the Dirac scalar part, related at large momenta to the perturbative running mass, is enhanced at low momenta, even in the chiral limit [31,32]: a demonstration of $D\chi SB$. One feature of this approach is that it allows one to make statements about light quarks, as opposed to the static potential of the Wilson loop. In SU(2) gauge theory the infrared properties of the quark propagator were found to be dominated by center vortices [25,33]. Unfortunately, the vortex picture for the gauge group SU(3) is less clear: while vortex removal eliminates the linear rise of the static quark potential at large distances, the string tension of vortex-only configurations falls short by roughly a factor of 2/3 [23,34,35].

To gain further insights into the SU(3) vortex picture, we here investigate the SU(3) quark propagator under the removal of center vortices. We will find that mass generation remains intact even after removing center vortices, while the string tension vanishes as expected.

II. CENTER VORTICES

We will identify center vortices in SU(3) Yang-Mills lattice gauge configurations using standard methods. Having generated gauge configurations, we will rotate them to direct maximal center gauge, then project the gauge links onto the nearest center element. Each configuration can then be decomposed into two pieces: the center element and “the rest.” An appealing result of such a decomposition would be the identification of separate short- and long-ranged pieces, such as are seen in SU(2) gauge theory [33]; that is, that this decomposition corresponds to a separation of infrared (vortex-only) and ultraviolet (vortex-removed) physics. Finally, to study the propagators, the vortex-only and vortex-removed configurations are rotated to Landau gauge and the quark propagators are calculated.

A statistical ensemble of lattice gauge configurations is generated using the Lüscher-Weisz [36] mean-field improved action,

$$S_G = \frac{5\beta}{3} \sum_{\text{sq}} \frac{1}{3} \text{Re tr}(1 - U_{\text{sq}}(x)) - \frac{\beta}{12u_0^2} \sum_{\text{rect}} \frac{1}{3} \text{Re tr}(1 - U_{\text{rect}}(x)),$$

where $U_{\text{sq}}(x)$ is the plaquette and $U_{\text{rect}}(x)$ denotes the rectangular 1×2 and 2×1 loops. For the tadpole improvement factor we employ the gauge-invariant plaquette measure

$$u_0 = \left(\frac{1}{3} \text{Re tr} \langle U_{\text{sq}} \rangle \right)^{1/4}. \quad (1)$$

A. Maximal center gauge

In order to identify the center fluxes of a given lattice configuration it is common to use gauge fixing and center projection. The center fluxes through an elementary plaquette are represented by center link elements $Z_\mu(x)$ which take values in the center group $Z_3 \subset SU(3)$:

$$Z_\mu(x) = \exp\left\{i \frac{2\pi}{3} m_\mu(x)\right\}, \quad m_\mu(x) \in \{-1, 0, 1\}.$$

It is a nontrivial task to find a definition of the center links that is sensible in the continuum limit. The following definition has turned out to be fruitful [11,17,23]:

$$\sum_{x,\mu} \|U_\mu^\Omega(x) - Z_\mu(x)\| \xrightarrow{\Omega, Z_\mu(x)} \min. \quad (2)$$

This has an intuitive interpretation: After a suitable gauge transformation $\Omega(x)$, we look for those center links $Z_\mu(x)$ that represent best a given link $U_\mu(x)$. Equation (1) implies that the overlap between the gauged links and the center links is maximized:

$$\sum_{x,\mu} \text{Re}[\text{Tr} U_\mu^\Omega(x) Z_\mu^\dagger(x)] \xrightarrow{\Omega, Z_\mu(x)} \max. \quad (3)$$

Hence, we will exploit the gauge degrees of freedom to bring $U_\mu^\Omega(x)$ as close as possible to a center element. Assuming that the deviations of $U_\mu^\Omega(x)$ from a center element are small, one might approximately solve (2) by setting

$$Z_\mu(x) \approx \frac{1}{3} \text{Tr} U_\mu^\Omega(x), \text{ or } Z_\mu(x) \approx \left[\frac{1}{3} \text{Tr} U_\mu^\Omega(x) \right]^2. \quad (4)$$

One gauge condition for determining the gauge transformation Ω is

$$R_{\text{mes}} = \sum_{x,\mu} |\text{Tr} U_\mu^\Omega(x)|^2 \xrightarrow{\Omega} \max. \quad (5)$$

This gauge conditions specifies a particular maximal center gauge, known in the literature as the ‘‘mesonic’’ center gauge [23,37,38].

B. Center projection and vortex removal

Once the optimal choice for the gauge transformation $\Omega(x)$ is obtained, the center links $Z_\mu(x)$ are obtained from the gauged links $U_\mu^\Omega(x)$ by center projection. Decomposing a particular link

$$\frac{1}{3} \text{Tr} U_\mu^\Omega(x) = r_\mu(x) \exp(i\varphi_\mu(x)), \quad (6)$$

where $r_\mu(x)$ is real and $\varphi_\mu(x) \in [-\pi, \pi)$, Eq. (3) implies that we locally maximize

$$\cos\left[\varphi_\mu(x) - \frac{2\pi}{3} m_\mu(x)\right] \xrightarrow{m_\mu} \max. \quad (7)$$

Hence, the integer $m_\mu(x) \in \{-1, 0, 1\}$ closest to $3\varphi_\mu(x)/2\pi$ is chosen. Once the center links $Z_\mu(x)$ are obtained in this way, center fluxes $\phi_{\mu\nu}(x)$ are detected from the center plaquettes

$$P_{\mu\nu}(x) = Z_\mu(x) Z_\nu(x + \mu) Z_\mu^\dagger(x + \nu) Z_\nu^\dagger(x) = \exp\left\{i \frac{2\pi}{3} \phi_{\mu\nu}(x)\right\}, \quad (8)$$

where

$$\phi_{\mu\nu}(x) \in \{-1, 0, 1\}.$$

We say that a particular plaquette $(\mu, \nu; x)$ is intersected by nontrivial center flux if $\phi_{\mu\nu}(x) \neq 0$. It can be shown, using the Z_3 Bianchi identity, that the set of plaquettes that carry nontrivial center flux form closed surfaces on the dual lattice. These surfaces define the world sheets of Z_3 vortices. The theory without center fluxes (vortex-removed configurations) is defined from the link elements

$$\tilde{U}_\mu(x) \equiv U_\mu^\Omega(x) Z_\mu^\dagger(x). \quad (9)$$

C. Numerical results

The configurations are fixed to maximal center gauge by maximizing the gauge-fixing functional (5) with the help of a local update algorithm. The algorithm is presented in detail in [38]. Lattice sizes and simulation parameters are listed in Table I.

In Fig. 1, we show the final value of the gauge-fixing functional R_{mes} for several values of the lattice spacing a . Generically, increasing values for R_{mes} are obtained for decreasing lattice spacing. This indicates that the overlap of the full configurations with pure center ones increases towards the continuum limit.

If ρ denotes the planar vortex area density then the quantity ρa^2 can be interpreted as the probability that a given plaquette carries nontrivial center flux. We have calculated ρa^2 for several lattice spacings (see Table I)

TABLE I. Simulation parameters β , volumes, string tension $a\sqrt{\sigma}$, lattice spacings a and vortex densities. The values for the lattice spacings for the $16^3 \times 32$ lattices have been obtained by using 50 configurations each. For the small $\beta = 4.60$ lattice estimates are taken from the larger lattice.

β	Volume	N_{con}	$a\sqrt{\sigma}$	a_σ [fm]	ρa^2	ρ/σ
4.10	$12^3 \times 24$	15	0.611(20)	0.272(9)	0.1414(4)	0.379(25)
4.38	$16^3 \times 32$	100	0.368(5)	0.165(3)	0.0539(2)	0.398(30)
4.53	$16^3 \times 32$	100	0.299(11)	0.134(5)	0.0339(2)	0.380(28)
4.60	$16^3 \times 32$	100	0.272(11)	0.122(5)	0.0281(2)	0.380(31)
4.60	$12^3 \times 24$	15	0.272(11)	0.122(5)	0.0289(5)	0.391(32)
4.80	$16^3 \times 32$	100	0.207(5)	0.093(2)	0.0173(2)	0.404(20)

by counting the number of plaquettes with nontrivial center fluxes and then dividing this number by the total number of plaquettes on the lattice. The interesting observation is that the planar vortex density, ρ , is independent of the lattice spacing a (Fig. 1) and therefore has a sensible continuum interpretation. This behavior is in accordance with the behavior of the SU(2) vortex density, and confirms earlier findings for the gauge group SU(3) [23].

Now, we calculate the static quark antiquark potential for ensembles with full SU(3) links, for vortex-only configurations and for vortex-removed configurations. As illustrated in Fig. 2, we observe that the vortex-removed configurations show no sign of a confining potential. On the other hand, the vortex-only ensembles give rise to around 60% of the string tension. This confirms earlier findings [23,34] and is in sharp contrast to the case of SU(2) gauge theory: there, the vortices reproduce a great deal of the full string tension [13].

III. QUARK PROPAGATOR ON THE LATTICE

In a covariant gauge in the continuum, Lorentz invariance allows us to decompose the full quark propagator into

Dirac vector and scalar pieces. In momentum space, the renormalized Euclidean space quark propagator has the form

$$S(\zeta; p) = \frac{1}{i\not{p}A(\zeta; p^2) + B(\zeta; p^2)} = \frac{Z(\zeta; p^2)}{i\not{p} + M(p^2)}, \quad (10)$$

where ζ is the renormalization point.

When the quark-gluon interactions are turned off, the quark propagator takes its tree-level form

$$S^{(0)}(p) = \frac{1}{i\not{p} + m}, \quad (11)$$

where m is the bare quark mass. When the interactions with the gluon field are turned on we have

$$S^{(0)}(p) \rightarrow S^{\text{bare}}(a; p) = Z_2(\zeta; a) S(\zeta; p), \quad (12)$$

where a is the regularization parameter (i.e., the lattice spacing) and $Z_2(\zeta; a)$ is the renormalization constant. In the MOM scheme it is chosen so as to ensure tree-level behavior at the renormalization point, $Z(\zeta; \zeta^2) = 1$. Note that $M(p^2)$ is renormalization point independent, i.e., since

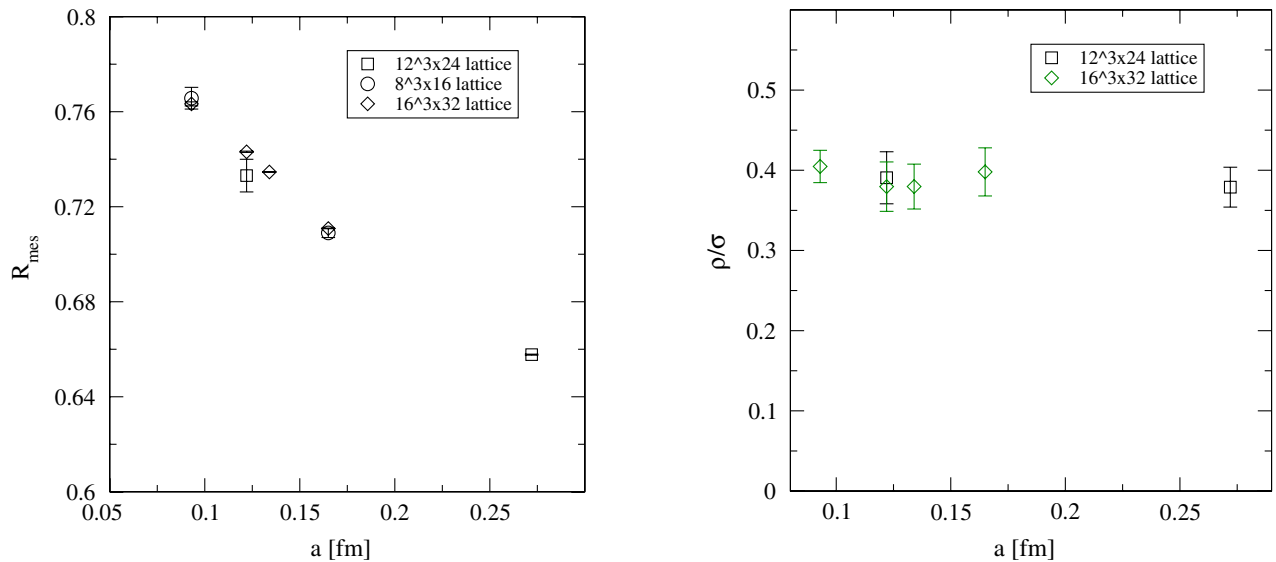


FIG. 1 (color online). Left panel: The gauge-fixing functional R_{mes} after MCG gauge fixing. Right panel: the vortex area density ρ in units of the string tension σ as function of the lattice spacing a .

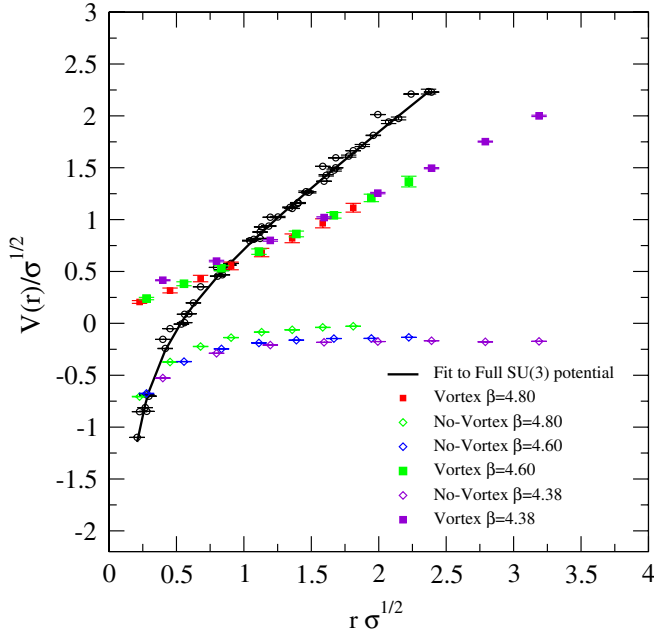


FIG. 2 (color online). The quark antiquark potential $V(r)$ as function of the quark antiquark distance r for full configurations (open circles), vortex-only configurations (full squares) and vortex-removed configurations (open diamonds).

$S(\zeta; p)$ is multiplicatively renormalizable all of the renormalization-point dependence is carried by $Z(\zeta; p^2)$. For simplicity of notation we suppress the a -dependence of the bare quantities.

In this work we use the AsqTad quark action [39] because of its excellent scaling and rotational symmetry properties [31]. The Dirac scalar and vector functions, $M(p^2)$ and $Z(p^2)$ are extracted from the propagator using the techniques described in detail in Ref. [40].

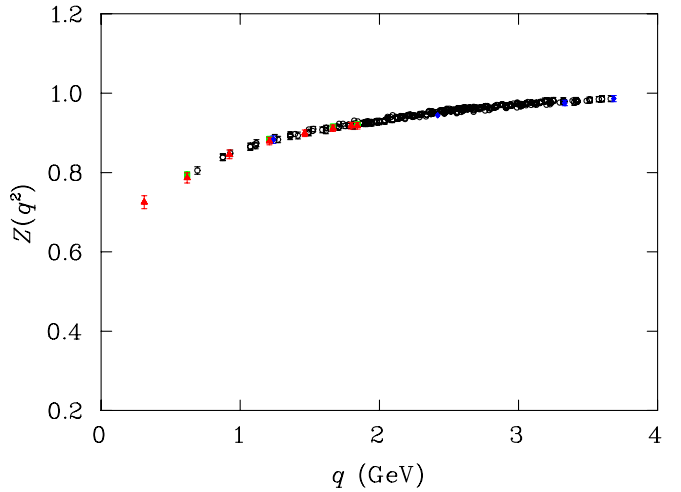
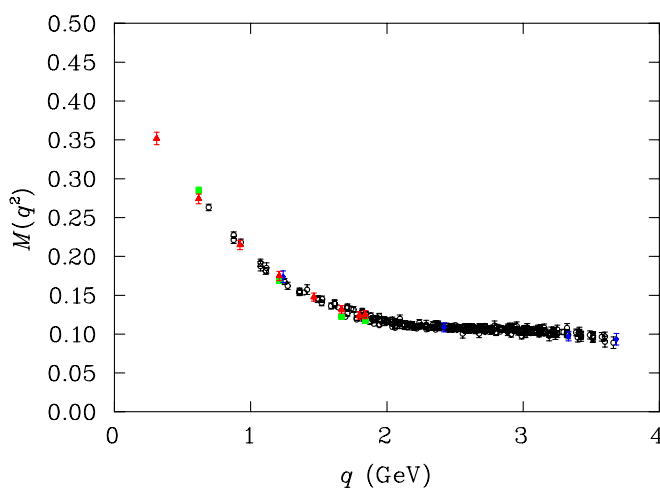


FIG. 3 (color online). The Landau-gauge quark propagator. The left panel shows the mass function $M(q^2)$ and the right panel the wave-function renormalization function $Z(q^2)$ for $m_0 a = 0.048$. The infrared enhancement of the mass function demonstrates $D\chi$ SB. Filled (red) triangles, (green) squares and (blue) diamonds denote momenta oriented along the time axis, a spatial axis, or the four-diagonal, respectively.

When analyzing our results we will sometimes find it convenient to use a “cylinder cut” [41], where we select only data with four-momentum lying near the four-dimensional diagonal. This is motivated by the observation that for a given momentum squared, (p^2), choosing the smallest momentum values of each of the Cartesian components, p_μ , should minimize finite lattice spacing artifacts. By eliminating points most likely to be affected by hyper-cubic lattice artifacts it is easier to draw robust conclusions.

IV. THE INFLUENCE OF CENTER VORTICES

The Landau-gauge quark propagator is calculated on the $16^3 \times 32$ configurations at $\beta = 4.60$. The quark mass and wave-function renormalization functions of the original untouched gauge configurations are illustrated in Fig. 3. Here symbols are used to identify momenta having a particular orientation within the lattice. Triangles denote momenta lying along the Cartesian time direction (the long dimension), squares denote momenta oriented along one spatial Cartesian direction, and diamonds denote momenta oriented along the lattice four-diagonal. A comparison of triangles and squares is useful in revealing finite volume effects at small momenta.

As is well known [26,31], the mass function is strongly enhanced in the infrared. This is true even in the chiral limit: a clear demonstration of dynamical chiral symmetry breaking. The infrared value of around 350 MeV is consistent with the constituent quark model. $Z(q^2)$ is somewhat suppressed in the infrared. A study on larger lattices reveals a flattening of both $M(q^2)$ and $Z(q^2)$ below around 500 MeV [42]. This is significant for confinement, because an Euclidean propagator cannot have a point of inflexion and adhere to reflection positivity [32].

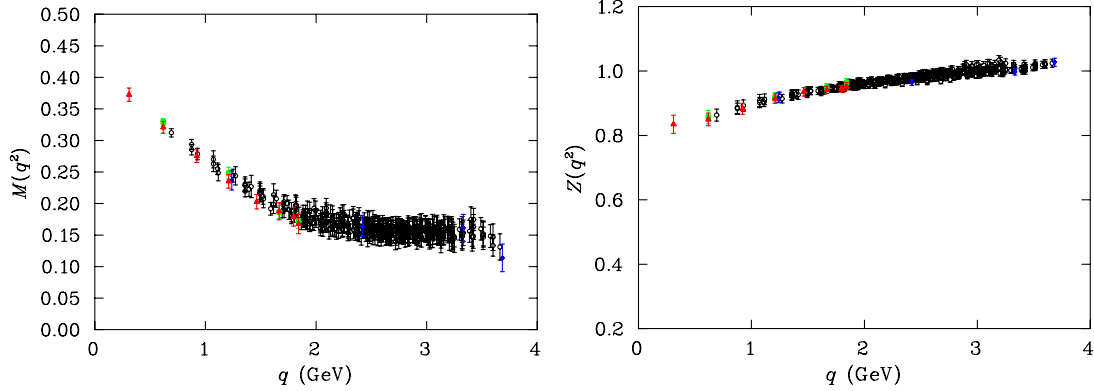


FIG. 4 (color online). Landau-gauge quark propagator for $m_0 a = 0.048$ following the removal of center vortices. $D\chi$ SB still clearly dominates the mass function. Both functions are somewhat flatter than on the full configurations. Symbols are as in Fig. 3.

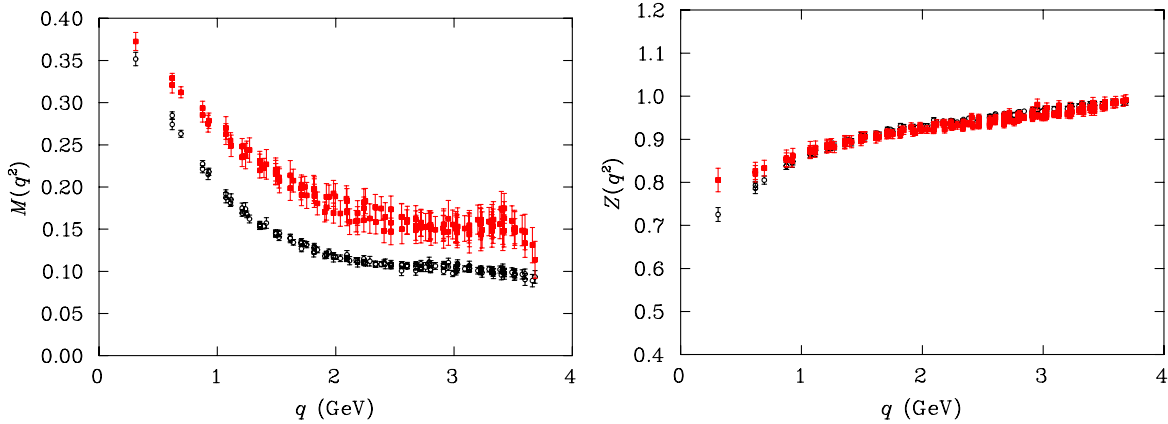


FIG. 5 (color online). Landau-gauge quark propagator for $m_0 a = 0.048$. Open circles denote the propagator obtained from the original gauge field configurations whereas the (red) filled squares denote the propagator following the removal of center vortices. $Z(q^2)$ is renormalized to one at the largest accessible momentum point.

Figure 4 shows the mass and wave-function renormalization functions after removing center vortices. Mass generation associated with dynamical chiral symmetry breaking is almost as strong after removing the center vortices as it was before. A roughening of the mass function at large momenta suggests that the removal of center vortices introduces significant noise into the gauge field configurations giving rise to a larger effective mass. $Z(p^2)$ is similarly weakly altered, being slightly noisier and having less infrared suppression than on the full configurations.

Figure 5 shows a direct comparison of the quark propagator on the full and vortex-removed configurations. Data has been cylinder cut to facilitate a detailed comparison. The wave-function renormalization function has been renormalized so that $Z(q^2) = 1$ at the largest momentum considered on the lattice. Only below about 1 GeV is there any significant difference between the full and vortex-removed results. It is possible that the removal of center vortices has caused $Z(p^2)$ to straighten out, which could restore reflection positivity and hence be a sign of deconfinement.

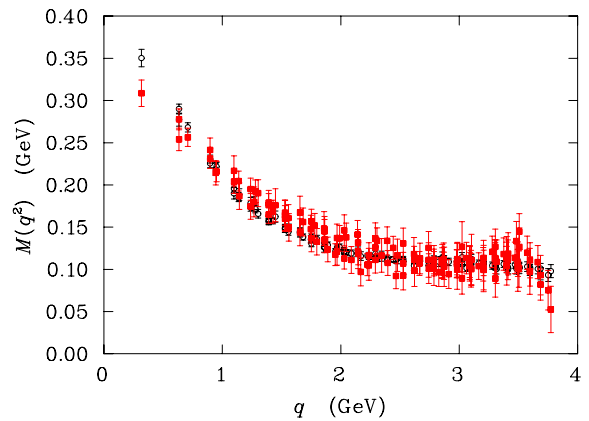


FIG. 6 (color online). The Landau-gauge quark propagator with $m_0 a = 0.048$ from the original configurations (open circles) is compared with the propagator obtained from the vortex-removed configurations with $m_0 a = 0.024$ (filled squares) selected to match the renormalized quark mass in the ultraviolet regime.

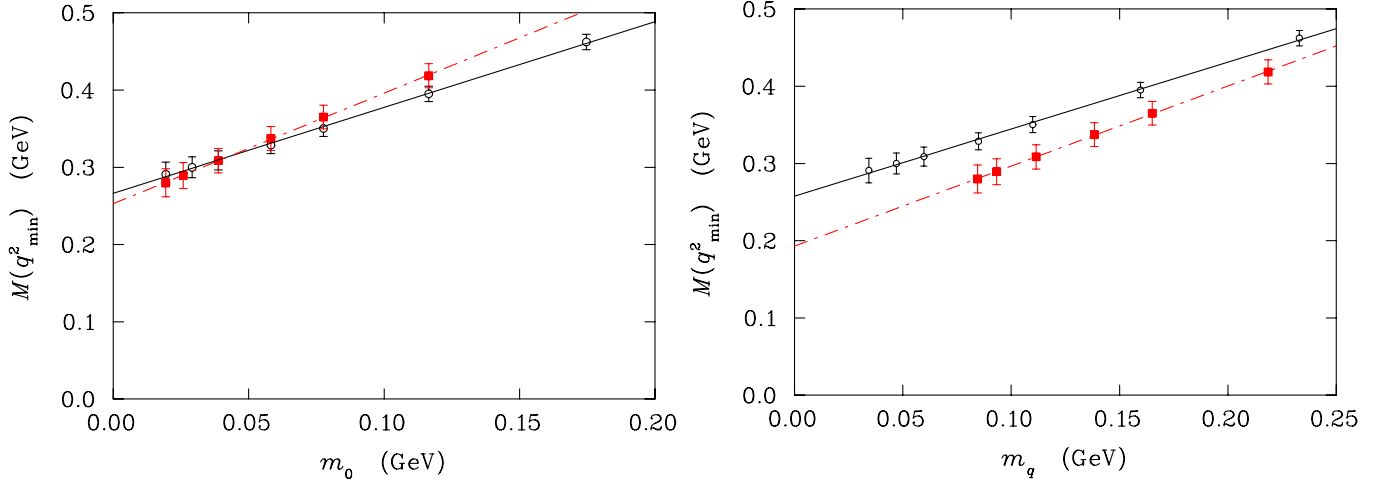


FIG. 7 (color online). Mass function at the smallest nontrivial momentum available on our lattice, $M(q_{\min}^2)$, for a variety of bare quark masses, m_0 . Open circles denote the mass function obtained from the original gauge field configurations whereas the (red) filled squares denote the mass function following the removal of center vortices. Original and vortex-removed results are compared for equal bare quark masses (left) and equal renormalized quark masses, m_q , at $q = 3.0$ GeV (right). The lines indicate linear fits to the data.

The mass function does not undergo a multiplicative renormalization, as described in Sec. III. However, removing the center vortices has significantly increased the running mass as displayed in the ultraviolet regime of the mass function. An alternative analysis is to compare full and vortex-removed results with bare quark masses adjusted to provide matched running quark masses. Figure 6 illustrates the persistent nature of the mass function under vortex removal. In this case we see that removing the vortices suppresses $M(q^2)$ near zero four-momentum by about 15% compared to the full configurations, weakening—but by no means eliminating—strong infrared enhancement. Either way, there is still plenty of dynamical mass generation.

To further explore the infrared nature of the quark mass function we turn our focus to the value of the mass function at the smallest nontrivial momentum available on our lattice, $q_{\min}^2 = 0.10$ GeV². Figure 7 compares the mass function at q_{\min}^2 for a variety of bare quark masses, m_0 . In the left-hand plot, $M(q_{\min}^2)$ is compared directly with the input bare quark mass, whereas the right hand plot compares $M(q_{\min}^2)$ with renormalized quark masses, m_q defined at $q = 3.0$ GeV. Linear fits are sufficient to describe the data and indicate significant dynamical mass generation in the chiral limit.

In the early days of Dyson-Schwinger studies of QCD, $D\chi$ SB was attributed to the interaction strength in the quark sector provided by an effective 1-gluon exchange. Although it is now clear [43] that vertex corrections play an important role in the quark IR sector, it is unlikely that a loss of gluonic interaction strength (as displayed by the full gluon propagator) goes unnoticed with regard to $D\chi$ SB. On the basis of our findings above, it is therefore interesting to study the effect of center vortex removal on the Landau-gauge gluon propagator.

As far as the full gluon propagator, $D(q^2)$, is concerned, it is known to be infrared enhanced, but finite at zero four-momentum [44–47]. This can be seen in Fig. 8 from the gluon dressing function, $q^2 D(q^2)$ of the Landau-gauge gluon propagator. At high momenta, the dressing function logarithmically decreases with momentum, while it is enhanced at intermediate momenta with a maximum near 1 GeV. The turnover indicates a violation of positivity, as explicitly shown in Ref. [28–30]. The same picture was found in full QCD with light sea quarks [30,48]. Also shown in Fig. 8 is the dressing function upon vortex

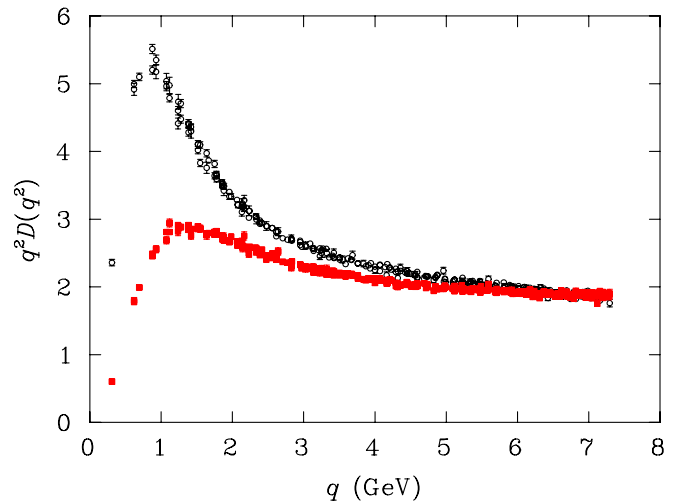


FIG. 8 (color online). The gluon propagator multiplied by q^2 (gluon dressing function) such that the large momentum value approaches a constant. The data presented here have been cylinder cut. Open circles denote results from the original untouched gauge fields while (red) full squares report the propagator after removing center vortices.

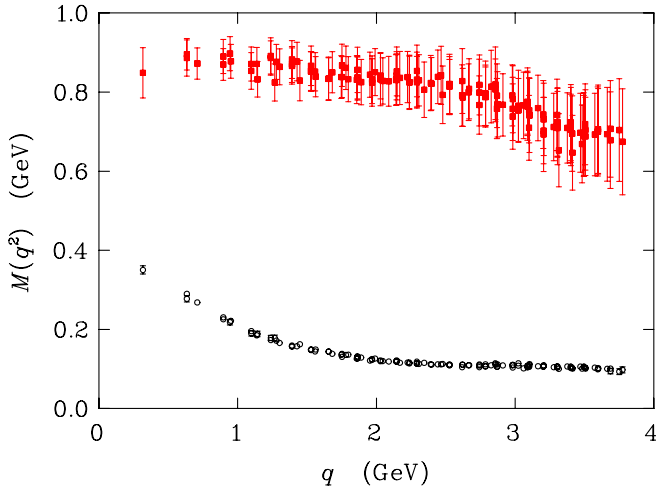


FIG. 9 (color online). Landau-gauge quark propagator for $m_0 a = 0.048$. Open circles denote the propagator obtained from the original gauge field configurations whereas the (red) filled squares denote the propagator following the removal of center vortices identified in Laplacian center gauge.

removal. As for the gauge group $SU(2)$ [49,50], we find that the infrared enhancement is largely suppressed when center vortices are removed. This is particularly remarkable in the light of our previous findings: vortex removal strongly reduces the gluonic interactions strength, but dynamical mass generation is largely unaffected.

On a final note, we have also investigated the role of center vortices defined using Laplacian center gauge (LCG) [51], where the Laplacian gauge construction removes the gauge-fixing ambiguity. While vortices defined this way do account for the full string tension, the vortex

density diverges in the continuum limit [23]. On a practical side, there is an abundance of LCG vortices in the vacuum. Upon removing these vortices the configurations become extremely rough.

While the flattening of the renormalized wave-function renormalization function highlighted in Fig. 5 is observed with larger statistical fluctuations, the mass function revealed following LCG-vortex removal bares little resemblance to the original mass function. It is also dominated by noise at all distance scales as illustrated in Fig. 9, where the scale has been adjusted to accommodate the results.

Still, one might be interested in examining the infrared behavior of the mass function as one approaches the chiral limit. Figure 10 illustrates the mass function at the smallest nontrivial momentum, $M(q_{\min}^2)$, for a variety of bare quark masses, m_0 . Open circles denote the mass function obtained from the original gauge field configurations whereas the filled squares denote the mass function following the removal of LCG center vortices. Original and vortex-removed results are compared for equal bare quark masses in the left plot and equal renormalized quark masses, m_q , at $q = 3.0$ GeV in the right plot. Figure 11 illustrates the LCG-vortex-removed data for equal renormalized quark masses, m_q , at the largest momentum explored, $q = 3.8$ GeV.

As in Fig. 7, the lines indicate linear fits to the data. Of particular interest is whether the trend of the LCG-vortex-removed data, when plotted as a function of the renormalized quark mass, is consistent with the restoration of chiral symmetry in the chiral limit; *i.e.* $M(q_{\min}^2) = 0$ at $m_q = 0$. The dot-dash curves in Figs. 10 and 11 illustrate linear fits to the LCG-vortex-removed points while the fine dash curve extrapolates the trend revealed by the four heaviest

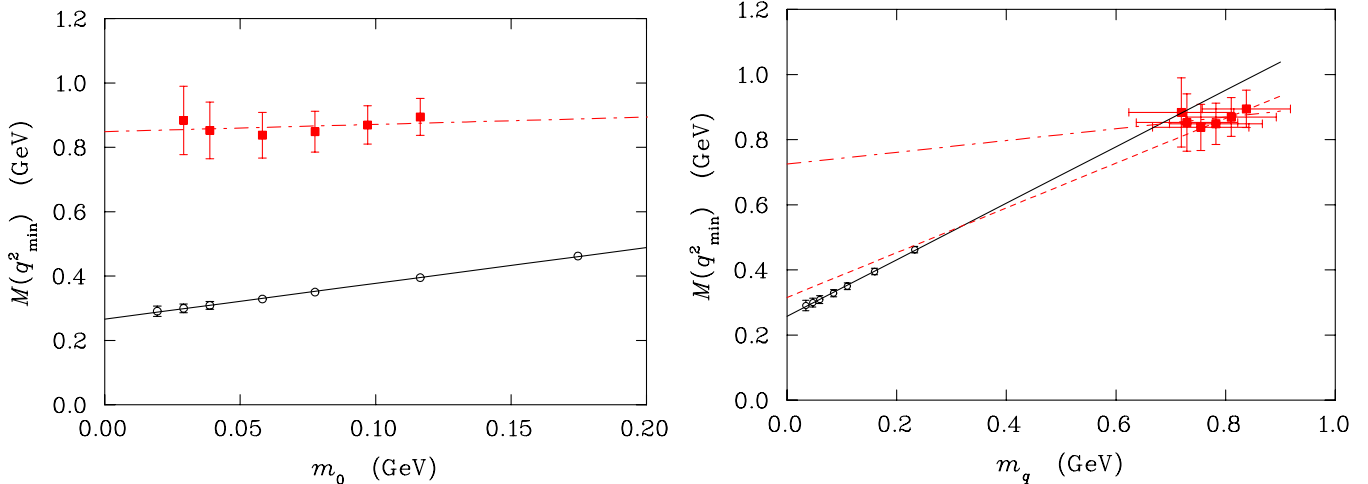


FIG. 10 (color online). Mass function at the smallest nontrivial momentum available on our lattice, $M(q_{\min}^2)$, for a variety of bare quark masses, m_0 . Open circles denote the mass function obtained from the original gauge field configurations whereas the (red) filled squares denote the mass function following the removal of LCG center vortices. Original and vortex-removed results are compared for equal bare quark masses (left) and equal renormalized quark masses, m_q , at $q = 3.0$ GeV (right). Lines indicate linear fits to the data as described in the text.

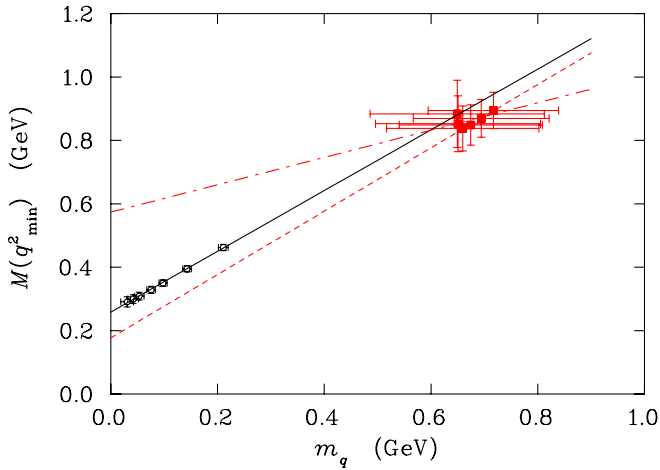


FIG. 11 (color online). Mass function at the smallest nontrivial momentum available on our lattice, $M(q_{\min}^2)$, plotted with respect to renormalized quark masses, m_q , defined at the largest momentum investigated; $q = 3.8$ GeV. Symbols are as in Fig. 10.

mass points. In either case, there is no evidence of a restoration of chiral symmetry in the LCG-vortex-removed mass function.

V. DISCUSSION

Using the SU(3) vortex picture defined by means of the mesonic version of the maximal center gauge [37,38] we have been able to construct a nonconfining version of QCD. As in the case of SU(2) gauge theory, an inspection of the gluonic dressing function shows a strong decline in the gluonic interaction strength. From this we might expect chiral symmetry restoration as well as deconfinement.

In contrast to this expectation, we find that the removal of center vortices from our configurations has done little to interfere with chiral symmetry breaking, as seen by the persistent infrared enhancement of the quark mass

function. The analogy to the SU(2) gauge group [33] is thus also broken: in SU(2), vortex removal implies the restoration of chiral symmetry [22–24].

One might conclude then, that the SU(2) confinement/D χ SB mechanism is in some essential way different from that in SU(3), but we stress that the key to SU(3) center vortex matter might not have been found yet, i.e., the way that we have defined the SU(3) vortices is perhaps deficient. In particular, the string tension vanishes on vortex-removed configurations, but only around two thirds of the full string tension is recovered on vortex-only configurations.

In SU(2) gauge theory the center vortex picture neatly decomposes the short-range from the long-range features of the gauge theory. This is not what we have observed in the SU(3) theory. Whether the phenomenon of D χ SB disentangles from quark confinement for the SU(3) gauge group or whether an improved definition of SU(3) vortex texture would recombine them needs further investigation. Yet our findings offer the intriguing possibility to separately trace out the impact of confinement and the impact of D χ SB on hadronic observables.

ACKNOWLEDGMENTS

POB acknowledges fruitful discussions with Craig Roberts and Peter Tandy. This research was undertaken on the NCI National Facility in Canberra, Australia, which is supported by the Australian Commonwealth Government. We also acknowledge eResearch SA for generous grants of supercomputing time which have enabled this project. This work was supported by the Australian Research Council. The work of POB was supported by the Marsden Fund of the RSNZ. AS acknowledges support from the European Union through the FP7-PEOPLE-2009-RG program (Grant No. 256594).

-
- [1] E. Laermann and O. Philipsen, *Annu. Rev. Nucl. Part. Sci.* **53**, 163 (2003).
 - [2] Y. Aoki, S. Borsanyi, S. Durr, Z. Fodor, S. D. Katz *et al.*, *J. High Energy Phys.* **06** (2009) 088.
 - [3] A. Bazavov, T. Bhattacharya, M. Cheng, N. Christ, C. DeTar *et al.*, *Phys. Rev. D* **80**, 014504 (2009).
 - [4] C. Gattringer, *Phys. Rev. Lett.* **97**, 032003 (2006).
 - [5] F. Bruckmann, C. Gattringer, and C. Hagen, *Phys. Lett. B* **647**, 56 (2007).
 - [6] F. Synatschke, A. Wipf, and C. Wozar, *Phys. Rev. D* **75**, 114003 (2007).
 - [7] F. Synatschke, A. Wipf, and K. Langfeld, *Phys. Rev. D* **77**, 114018 (2008).
 - [8] A. S. Kronfeld, M. L. Laursen, G. Schierholz, and U. J. Wiese, *Phys. Lett. B* **198**, 516 (1987).
 - [9] T. Suzuki and I. Yotsuyanagi, *Phys. Rev. D* **42**, 4257 (1990).
 - [10] H. Suganuma, S. Sasaki, and H. Toki, *Nucl. Phys.* **B435**, 207 (1995).
 - [11] L. Del Debbio, M. Faber, J. Greensite, and S. Olejnik, *Phys. Rev. D* **55**, 2298 (1997).
 - [12] L. Del Debbio, M. Faber, J. Giedt, J. Greensite, and S. Olejnik, *Phys. Rev. D* **58**, 094501 (1998).
 - [13] J. Greensite, *Prog. Part. Nucl. Phys.* **51**, 1 (2003).
 - [14] G. 't Hooft, *Nucl. Phys.* **B138**, 1 (1978).
 - [15] G. 't Hooft, *Nucl. Phys.* **B153**, 141 (1979).
 - [16] L. Del Debbio, M. Faber, J. Greensite, and S. Olejnik, *Nucl. Phys. B, Proc. Suppl.* **53**, 141 (1997).
 - [17] K. Langfeld, H. Reinhardt, and O. Tennert, *Phys. Lett. B* **419**, 317 (1998).

- [18] K. Langfeld, O. Tennert, M. Engelhardt, and H. Reinhardt, *Phys. Lett. B* **452**, 301 (1999).
- [19] M. Engelhardt, K. Langfeld, H. Reinhardt, and O. Tennert, *Phys. Rev. D* **61**, 054504 (2000).
- [20] K. Langfeld, *Phys. Rev. D* **67**, 111501 (2003).
- [21] P. de Forcrand and L. von Smekal, *Phys. Rev. D* **66**, 011504 (2002).
- [22] P. de Forcrand and M. D'Elia, *Phys. Rev. Lett.* **82**, 4582 (1999).
- [23] K. Langfeld, *Phys. Rev. D* **69**, 014503 (2004).
- [24] J. Gattnar *et al.*, *Nucl. Phys.* **B716**, 105 (2005).
- [25] R. Hollwieser, M. Faber, J. Greensite, U. M. Heller, and S. Olejnik, *Phys. Rev. D* **78**, 054508 (2008).
- [26] R. Alkofer and L. von Smekal, *Phys. Rep.* **353**, 281 (2001).
- [27] C. S. Fischer, *J. Phys. G* **32**, R253 (2006).
- [28] A. Cucchieri, T. Mendes, and A. R. Taurines, *Phys. Rev. D* **71**, 051902 (2005).
- [29] A. Sternbeck, E. M. Ilgenfritz, M. Müller-Preussker, A. Schiller, and I. L. Bogolubsky, *Proc. Sci., LAT2006* (2006) 076.
- [30] P. O. Bowman *et al.*, *Phys. Rev. D* **76**, 094505 (2007).
- [31] P. O. Bowman, U. M. Heller, D. B. Leinweber, A. G. Williams, and J. B. Zhang, *Lect. Notes Phys.* **663**, 17 (2005).
- [32] C. D. Roberts, *Prog. Part. Nucl. Phys.* **61**, 50 (2008).
- [33] P. O. Bowman *et al.*, *Phys. Rev. D* **78**, 054509 (2008).
- [34] A. O. Cais *et al.*, *Proc. Sci., LAT2007* (2007) 321.
- [35] A. O'Cais *et al.*, *Phys. Rev. D* **82**, 114512 (2010).
- [36] M. Lüscher and P. Weisz, *Commun. Math. Phys.* **97**, 59 (1985).
- [37] M. Faber, J. Greensite, and S. Olejnik, *Phys. Lett. B* **474**, 177 (2000).
- [38] A. Montero, *Phys. Lett. B* **467**, 106 (1999).
- [39] K. Orginos, D. Toussaint, and R. L. Sugar (MILC), *Phys. Rev. D* **60**, 054503 (1999).
- [40] P. O. Bowman *et al.*, *Phys. Rev. D* **71**, 054507 (2005).
- [41] D. B. Leinweber, J. I. Skullerud, A. G. Williams, and C. Parrinello (UKQCD), *Phys. Rev. D* **58**, 031501 (1998).
- [42] M. B. Parappilly *et al.*, *Phys. Rev. D* **73**, 054504 (2006).
- [43] R. Alkofer, C. S. Fischer, and F. J. Llanes-Estrada, *Phys. Lett. B* **611**, 279 (2005).
- [44] F. D. R. Bonnet, P. O. Bowman, D. B. Leinweber, A. G. Williams, and J. M. Zanotti, *Phys. Rev. D* **64**, 034501 (2001).
- [45] A. Sternbeck, L. von Smekal, D. B. Leinweber, and A. G. Williams, *Proc. Sci., LAT2007* (2007) 340.
- [46] A. Cucchieri and T. Mendes, *Phys. Rev. Lett.* **100**, 241601 (2008).
- [47] I. L. Bogolubsky, E. M. Ilgenfritz, M. Müller-Preussker, and A. Sternbeck, *Phys. Lett. B* **676**, 69 (2009).
- [48] P. O. Bowman, U. M. Heller, D. B. Leinweber, M. B. Parappilly, and A. G. Williams, *Phys. Rev. D* **70**, 034509 (2004).
- [49] K. Langfeld, H. Reinhardt, and J. Gattnar, *Nucl. Phys. B* **621**, 131 (2002).
- [50] J. Gattnar, K. Langfeld, and H. Reinhardt, *Phys. Rev. Lett.* **93**, 061601 (2004).
- [51] P. de Forcrand and M. Pepe, *Nucl. Phys.* **B598**, 557 (2001).